ChemComm

COMMUNICATION

View Article Online
View Journal | View Issue

Cite this: *Chem. Commun.*, 2016, 52, 11500

Received 14th July 2016,
Accepted 30th August 2016

DOI: 10.1039/c6cc05810h

www.rsc.org/chemcomm

A high performance three-dimensional thiophene-annulated perylene dye as an acceptor for organic solar cells†

Wei Fan,‡[ab] Ningning Liang,‡[ab] Dong Meng,[ab] Jiajing Feng,[ab] Yan Li,*[a] Jianhui Hou[a] and Zhaohui Wang[a]

A high performance three-dimensional (3D) thiophene-annulated perylene dye, namely tetra-PBI-S, was designed and synthesized. The appropriate LUMO level, balanced carrier mobilities and favourable phase separation make tetra-PBI-S based solar cells show a much higher power conversion efficiency (PCE) of 6.2% than tetra-PBI based solar cells with a PCE of 3.6%.

Bulk-heterojunction (BHJ) organic solar cells based on non-fullerene acceptors have attracted much attention due to their advantages such as easily tunable energy levels, excellent optical absorption properties, and potential for low-cost and large-area production.[1] Recently, the rapid development of non-fullerene acceptors applied in BHJ organic solar cells rewrote a series of power conversion efficiency (PCE) records.[2] Among the manifold non-fullerene acceptors, perylene bisimide derivatives (PBIs) were some of the earliest and most common acceptors studied in BHJ organic solar cells because of their strong absorption ability, high electron mobility, and durability to light and temperature.[3] To suppress the aggregation of PBI-based acceptors, a non-planar perylene architecture emerges as the most efficient design concept. For example, functionalization of perylene cores by sterically hindered substitutions in the bay or nonbay regions could prevent the aggregation in the solid state.[4] On the other hand, developing new PBI-based molecular structures such as PBI oligomers linked in the bay, non-bay region or imide groups was considered as a more effective way to reduce intermolecular aggregation.[5] Recently, Yan developed a series of tetraphenyl carbon-group core based PBIs in which four PBI units linked with tetraphenylmethane, tetraphenylsilane and tetraphenylgermane cores, respectively.[6] Though these small molecular acceptors have the three-dimensional (3D) ball-shaped structure of fullerenes, they still displayed relatively low PCEs.

We are particularly interested in heteroatom-annulated polycyclic aromatic hydrocarbons.[7] In our previous work, bowl-shaped bis(perylene bisimide)s were successfully constructed by incorporating heteroatoms into the carbon skeleton as a result of the strain of five-membered heterorings.[8] The integration of heteroatoms into the molecular skeleton can not only change the original structures due to the strain of heterorings but also modulate intermolecular interactions such as van der Waals and heteroatom–heteroatom interactions, which are essential for achieving excellent device performance. Recently, a bay-linked perylene bisimide acceptor named SdiPBI was reported by us. Organic solar cells based on the SdiPBI acceptor show a high PCE of 5.9%.[9] Furthermore, we insert S atoms and Se atoms into the bay region of SdiPBI, affording two new compounds SdiPBI-S and SdiPBI-Se. The PCEs of solar cells based on them are up to 7.2% and 8.5%, respectively.[10] Inspired by our design strategy, herein we designed and synthesized a new 3D thiophene-annulated perylene dye, namely tetra-PBI-S, *via* incorporating S-atoms into the bay region of PBI subunits. As shown in Fig. 1, tetra-PBI-S has a tetrahedral configuration just like tetra-PBI. However, the integration of thiophene annulation in the bay region makes PBI subunits have a more planar skeleton, which may facilitate electron transport. Because of the electron-donating ability of the thiophene unit, tetra-PBI-S has a higher lying LUMO energy than tetra-PBI, which is favourable for improving the open-circuit voltage (V_{oc}). The combined properties such as the appropriate LUMO level, balanced carrier mobilities and favourable phase separation in BHJ films make organic solar cells based on the tetra-PBI-S acceptor show a much higher power conversion efficiency (PCE) of 6.2% than tetra-PBI-based solar cells with a PCE of 3.6%.

The synthetic route to tetra-PBI-S is shown in Scheme 1, and tetra-PBI with the same alkyl chain as that of tetra-PBI-S is synthesized according to ref. 6. S-Annulated PBI **2** was obtained in high yield by a surprisingly simple one-pot procedure from the readily available precursor 1-nitroperylene bisimide **1** that was synthesized by nitrification of PBI.[10b] This key step was carried out in *N*-methylpyrrolidone (NMP) with the sulfur powder at 190 °C following purification by column chromatography. The key

[a] *Beijing National Laboratory for Molecular Science, Institute of Chemistry, Chinese Academy of Sciences, Beijing 100190, China. E-mail: yanli@iccas.ac.cn*
[b] *University of Chinese Academy of Sciences, Beijing 100049, China*

† Electronic supplementary information (ESI) available. See DOI: 10.1039/c6cc05810h

‡ These authors contributed equally.

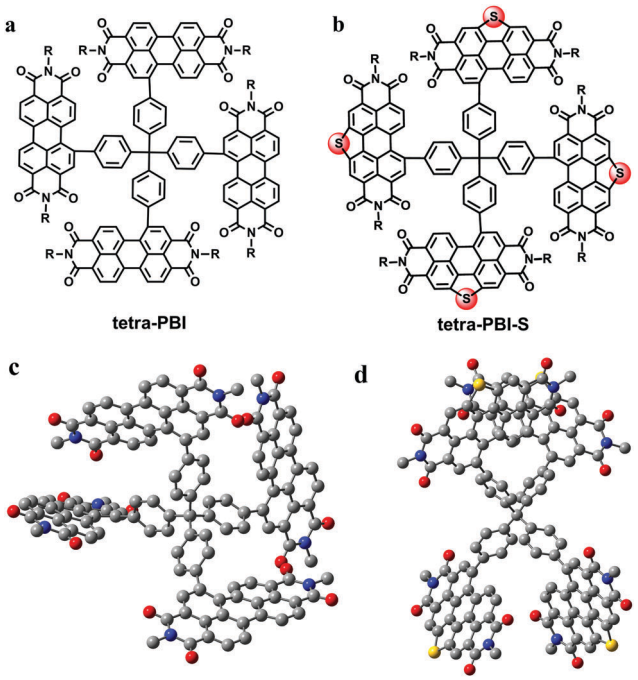

Fig. 1 Molecular structures: (a) tetra-PBI and (b) tetra-PBI-S. Optimized conformations of the two molecules: (c) tetra-PBI and (d) tetra-PBI-S.

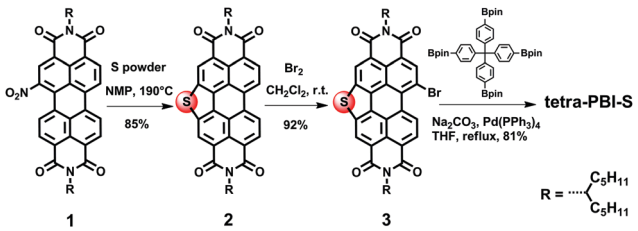

Scheme 1 Synthetic route to tetra-PBI-S.

intermediate **3** was synthesized by bromination of compound **2** in dichloromethane solvent at room temperature for 2 hours. The target molecule tetra-PBI-S was synthesized *via* Suzuki cross coupling reaction between brominated PBI-S **3** and tetrakis-[4-(4′,4′,5′,5′-tetramethyl-1′,3′,2′,-dioxaborolanephenyl)]methane. These compounds were fully characterized by ^{1}H and ^{13}C NMR spectroscopy and high-resolution mass spectrometry (HRMS). Tetra-PBI and tetra-PBI-S are highly soluble in common organic solvents such as dichloromethane and tetrahydrofuran due to their non-planar 3D structures and long branched alkyl chains.

The optimized geometries of tetra-PBI and tetra-PBI-S were calculated by using the density functional theory (DFT) at the B3LYP/6-31G(d,p) level. In order to facilitate the calculation, the long branched chains at the imide positions were replaced with methyl groups. As shown in Fig. 1, the PBI subunits of tetra-PBI are twisted and disperse evenly surrounding the tetraphenylmethane core as a well-shaped tetrahedral configuration. The dihedral angle between the PBI subunit and phenyl is about 56° (Fig. S1, ESI†). While in the molecular configuration of tetra-PBI-S, the inserted S atoms locked the bay regions to make PBI subunits have a planar skeleton. Meanwhile, the S-bridge

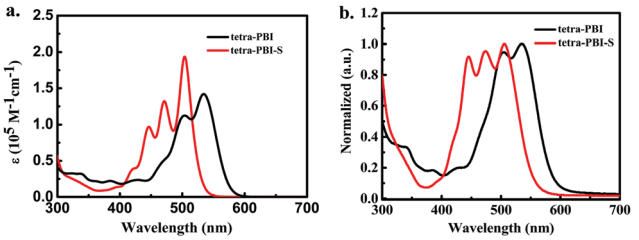

Fig. 2 UV-vis absorption spectra of tetra-PBI and tetra-PBI-S (a) in chloroform solution and (b) in films.

also makes the PBI subunits more rigid with a dihedral angle between the PBI and phenyl of about 76°. The entire molecular configuration of tetra-PBI-S is irregular compared with that of tetra-PBI as a result of large steric repulsion.

The UV-vis absorption spectra of tetra-PBI and tetra-PBI-S in dilute chloroform (1×10^{-5} M) and solid thin films are shown in Fig. 2. Tetra-PBI exhibits a broad absorption in the wavelength range between 450 nm and 600 nm with a maximum extinction coefficient of 1.43×10^{5} M^{-1} cm^{-1} at 534 nm. By contrast, tetra-PBI-S shows a blue-shifted and broad absorption throughout the 400–550 nm with a maximum extinction coefficient of 1.92×10^{5} M^{-1} cm^{-1} at 504 nm. The absorption spectra of tetra-PBI and tetra-PBI-S in solid films have similar low-energy maxima to those in solution, demonstrating that they all have weak aggregation in the solid state. As illustrated in Fig. S2 (ESI†), both the absorption spectra of tetra-PBI and tetra-PBI-S are complementary to that of PBDT-TS1, which is commonly used as a polymer donor in BHJ solar cells. The optimal band gaps (E_g^{opt}) of tetra-PBI and tetra-PBI-S estimated from the film absorption edges are 2.09 eV and 2.24 eV, respectively.

Electrochemical cyclic voltammetry (CV) was used to study the energy levels (Fig. S3, ESI†). As shown in Table 1, the LUMO and HOMO energy levels of tetra-PBI are −3.74 and −5.90 eV, respectively. The LUMO and HOMO energy levels of tetra-PBI-S are −3.68 and −6.02 eV, respectively. A higher LUMO energy level of tetra-PBI-S results from the strong donating ability of sulfur atoms.[10a] Referring to the LUMO and HOMO energy levels of donor material PBDT-TS1 (LUMO = −3.52 eV, HOMO = −5.33 eV), the energy offset between the HOMO of PBDT-TS1 and the LUMO of tetra-PBI-S is 1.56 eV to afford a high V_{oc}.

In order to investigate the photovoltaic properties, organic solar cells were fabricated with an inverted device architecture of ITO/ZnO/PBDT-TS1:acceptor/MoO_3/Al, where ITO is indium tin oxide, ZnO and MoO_3 were used as the n and p-type interfacial layers,

Table 1 Optical and electronic properties of tetra-PBI and tetra-PBI-S

	λ_{max}^{abs} [nm] [a]	λ_{max}^{film} [nm]	E_{HOMO} [b] [eV]	E_{LUMO} [c] [eV]	E_g [d] [eV]
Tetra-PBI	534	538	−5.90	−3.74	2.16
Tetra-PBI-S	504	506	−6.02	−3.68	2.34

[a] Measured in dilute $CHCl_3$ solution (1.0×10^{-5} M). [b] HOMO (eV) calculated according to $E_{HOMO} = (E_{LUMO} - E_g)$ eV. [c] LUMO (eV) estimated from the onset potential of the first reduction wave and calculated according to $E_{LUMO} = -(4.8 + E_{onset}^{re})$ eV. [d] Calculated by the onset edge of the absorption spectra in $CHCl_3$ solution according to $E_g = (1240/\lambda_{onset})$.

respectively, to facilitate charge transport and collection. Firstly, PBDT-TS1 : tetra-PBI-S mass blend ratios from 2 : 1 to 1 : 2 were tested to study the effect of the donor to acceptor weight ratio on device performance. The device parameters are summarized in Table S1 (ESI†). The current density–voltage (J–V) curves of the devices and the external quantum efficiency (EQE) spectra are shown in Fig. S5 (ESI†), respectively. A donor to acceptor weight ratio of 1 : 1.5 shows the best performance with V_{oc} = 0.965 V, J_{sc} = 11.97 mA cm^{-2}, FF = 43.3% and PCE = 5.0%. To further promote the device performance, di-phenyl ether (DPE) was used as a processing additive. The device performance parameters of PSCs based on the 1 : 1.5 blend ratio with different amounts of DPE are shown in Table S2 (ESI†), while the counterpart J–V curves of the devices and EQE spectra are shown in Fig. S6 (ESI†). When the concentration of DPE is 1%, the V_{oc} is similar to the cells without the additive, but the J_{sc} and FF are increased. Upon increasing the DPE concentration from 1% to 3%, the solar cells show slightly decreased V_{oc}, but increased J_{sc} and FF, to get a high PCE of 6.17%. Yet, the efficiency does not keep up with the 5% DPE additive on account of the decrease of V_{oc}, J_{sc} and FF. At the same time, solar cells based on the tetra-PBI acceptor were fabricated as a parallel experiment to study the effect without sulfur atoms in acceptor molecules. The compared device performance parameters based on the two acceptors are summarized in Table 2. Without the additive DPE for the tetra-PBI acceptor, the solar cells show a low PCE of 3.3% with V_{oc} = 0.952 V, J_{sc} = 9.27 mA cm^{-2}, and FF = 37.43%. When the DPE concentration is 3%, the J_{sc} and FF slightly increased, with a PCE of 3.6%, which still remains far below the tetra-PBI-S-based solar cells. The J–V curves and EQE spectra with the two acceptors are shown in Fig. 3. Both the solar cells based on the two acceptors show broad EQE spectra from 300 nm to 800 nm. The tetra-PBI-based solar cells have the maximum peak up to 40% at 530 nm, while the tetra-PBI-S-based solar cells have the maximum peak of 55% at 650 nm. The calculated J_{sc} values from EQE spectra for tetra-PBI and tetra-PBI-S are 8.91 mA cm^{-2} and 11.98 mA cm^{-2}, respectively.

To understand the charge transport properties of the devices under the optimal conditions, the space-charge-limited current (SCLC) method was used to measure the hole and electron mobilities with the device structure of ITO/PEDOT:PSS/PBDT-TS1:acceptor/Au and ITO/ZnO/PBDT-TS1:acceptor/Al, respectively. As shown in Table S3 and Fig. S7 (ESI†), the electron mobility based on the tetra-PBI-S blend film without the additive is 3.8×10^{-6} cm^2 V^{-1} s^{-1}. When 3% DPE was added, the electron mobility increased to 9.6×10^{-6} cm^2 V^{-1} s^{-1}. The corresponding hole mobility did not change apparently from 6.4×10^{-5} cm^2 V^{-1} s^{-1} to 5.8×10^{-5} cm^2 V^{-1} s^{-1}. The carrier mobilities of the tetra-PBI-S blend film with 3% DPE are all higher than those based on the tetra-PBI blend film, which has $\mu_e = 1 \times 10^{-6}$ cm^2 V^{-1} s^{-1} and $\mu_h = 2.7 \times 10^{-5}$ cm^2 V^{-1} s^{-1}. Besides, the tetra-PBI-S blend film with 3% DPE has more balanced carrier transport with μ_h/μ_e = 6. The high charge carrier mobility and balanced carrier transport would partially explain the high J_{sc} and high FF observed in tetra-PBI-S blend film based devices.

In order to research the effect of the additive on device performance, atomic force microscopy (AFM) was used to study the morphologies of PBDT-TS1:acceptor blend films. As shown in Fig. 4, the surface of the PBDT-TS1:tetra-PBI blend film without DPE is similar to the blend film including the 3% DPE additive. The two blend films have a root-mean-square (RMS) roughness of 0.75 nm and 0.78 nm, respectively. The additive has no obvious effect on phase separation for the tetra-PBI blend film. However, when the PBDT-TS1:tetra-PBI-S blend film was added with the 3% DPE additive, the RMS roughness changed apparently from 0.84 nm to 1.66 nm. It indicates that the addition of DPE may contribute to obtaining a favourable morphology to promote the phase separation and charge transport for the PBDT-TS1:tetra-PBI-S blend film.

Table 2 Device performance parameters of BHJ solar cells with 3% DPE or without under AM 1.5G illumination at 100 mW cm^{-2}

Blend	DPE [v/v, %]	V_{oc} [V]	J_{sc} [mA cm^{-2}]	FF [%]	PCE [%]
PBDT-TS1:tetra-PBI-S	0	0.966	11.95	43.32	5.00
	3	0.947	13.02	50.00	6.17
PBDT-TS1:tetra-PBI	0	0.952	9.27	37.43	3.30
	3	0.943	9.65	39.79	3.62

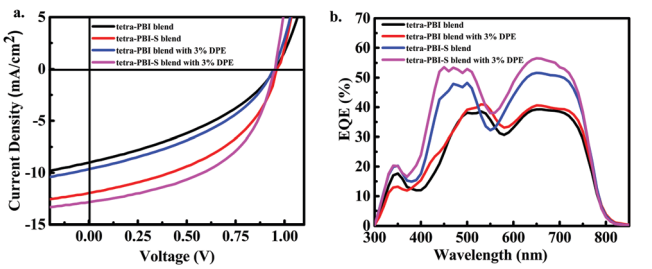

Fig. 3 (a) J–V characteristics and (b) EQE characteristics of OPV devices.

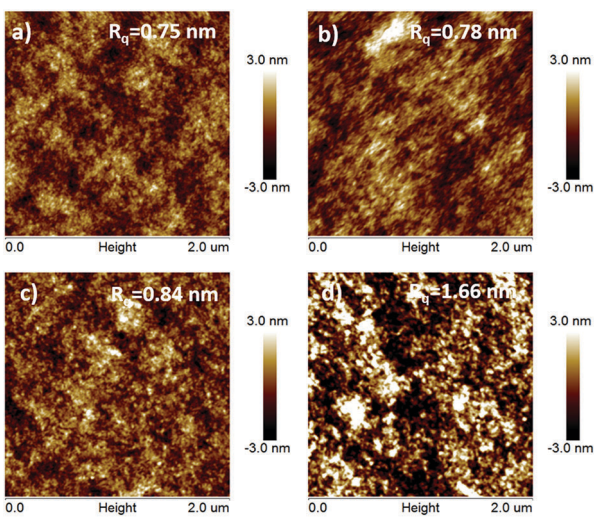

Fig. 4 AFM topographic images (2 μm × 2 μm) of tetra-PBI blend films (a) without and (b) with 3% DPE, and tetra-PBI-S blend films (c) without and (d) with 3% DPE.

To further investigate the different photovoltaic performances of the two non-fullerene acceptors, we carried out the grazing-incidence wide-angle X-ray scattering (GIWAXS) measurements to reveal the molecular packing of the two different 3D dyes. As shown in Fig. S8 (ESI†), for the tetra-PBI blend film with 3% DPE, the π–π stacking was not observed in the out-of-plane direction. However, there was a π–π stacking peak (q = 1.57 Å^{-1}, d = 4.01 Å) for the tetra-PBI-S blend film with 3% DPE, demonstrating that the tetra-PBI-S blend film with 3% DPE has a better molecular orientation on the face-on direction to facilitate vertical charge transport. Thus, it may also partially explain the higher J_{sc} of the tetra-PBI-S blend film compared with the tetra-PBI blend film.

In summary, a new high-performance 3D non-fullerene acceptor, namely tetra-PBI-S, was designed, synthesized and characterized. Compared with tetra-PBI, the integration of thiophene annulation in the bay region makes tetra-PBI-S have more planar PBI subunits, which may facilitate electron transport. Moreover, because of the electron-donating ability of the thiophene unit, tetra-PBI-S has a higher lying LUMO energy than tetra-PBI, which is favourable for improving V_{oc}. The combined properties such as the appropriate LUMO level, balanced carrier mobilities and favourable phase separation in the BHJ films make organic solar cells based on the tetra-PBI-S acceptor show a much higher power conversion efficiency (PCE) of 6.2% than tetra-PBI based solar cells with a PCE of 3.6%. The great promotion of device performance for the tetra-PBI-S acceptor provides a new design strategy to obtain high-performance acceptors for organic solar cells.

This work was financially supported by the National Natural Science Foundation of China (NSFC) (No. 21225209, 21190032), NSFC-DFG joint project TRR61 (21261130581), and the Chinese Academy of Sciences (XDB12010100). We gratefully acknowledge Prof. Z. Wei for the assistance with 2D GIWAXS measurements.

Notes and references

1 (*a*) C. B. Nielsen, S. Holliday, H.-Y. Chen, S. J. Cryer and I. McCulloch, *Acc. Chem. Res.*, 2015, **48**, 2803–2812; (*b*) L. Schmidt-Mende, A. Fechtenkötter, K. Müllen, E. Moons, R. H. Friend and J. D. MacKenzie, *Science*, 2001, **293**, 1119–1122; (*c*) D. Zhao, Q. Wu, Z. Cai, T. Zheng, W. Chen, J. Lu and L. Yu, *Chem. Mater.*, 2016, **28**, 1139–1146; (*d*) Q. Yan, Y. Zhou, Y.-Q. Zheng, J. Pei and D. Zhao, *Chem. Sci.*, 2013, **4**, 4389–4394; (*e*) Y. Zhou, L. Ding, K. Shi, Y.-Z. Dai, N. Ai, J. Wang and J. Pei, *Adv. Mater.*, 2012, **24**, 957–961; (*f*) Y.-J. Hwang, H. Li, B. A. E. Courtright, S. Subramaniyan and S. A. Jenekhe, *Adv. Mater.*, 2016, **28**, 124–131.

2 (*a*) L. Ye, W. Jiang, W. Zhao, S. Zhang, Y. Cui, Z. Wang and J. Hou, *Org. Electron.*, 2015, **17**, 295–303; (*b*) Y. Lin, Q. He, F. Zhao, L. Huo, J. Mai, X. Lu, C.-J. Su, T. Li, J. Wang, J. Zhu, Y. Sun, C. Wang and X. Zhan, *J. Am. Chem. Soc.*, 2016, **138**, 2973–2976; (*c*) H. Bin, Z.-G. Zhang, L. Gao, S. Chen, L. Zhong, L. Xue, C. Yang and Y. Li, *J. Am. Chem. Soc.*, 2016, **138**, 4657–4664; (*d*) W. Zhao, D. Qian, S. Zhang, S. Li, O. Inganäs, F. Gao and J. Hou, *Adv. Mater.*, 2016, **28**, 4734–4739.

3 (*a*) Z. Chen, A. Lohr, C. R. Saha-Möller and F. Würthner, *Chem. Soc. Rev.*, 2009, **38**, 564–584; (*b*) W. Jiang, Y. Li and Z. Wang, *Acc. Chem. Res.*, 2014, **47**, 3135–3147; (*c*) M. Ball, Y. Zhong, Y. Wu, C. Schenck, F. Ng, M. Steigerwald, S. Xiao and C. Nuckolls, *Acc. Chem. Res.*, 2015, **48**, 267–276; (*d*) T. Weil, T. Vosch, J. Hofkens, K. Peneva and K. Müllen, *Angew. Chem., Int. Ed.*, 2010, **49**, 9068–9093.

4 (*a*) Y. Cai, L. Huo, X. Sun, D. Wei, M. Tang and Y. Sun, *Adv. Energy Mater.*, 2015, **5**, 1500032; (*b*) P. E. Hartnett, A. Timalsina, H. S. S. Ramakrishna Matte, N. Zhou, X. Guo, W. Zhao, A. Facchetti, R. P. H. Chang, M. C. Hersam, M. R. Wasielewski and T. J. Marks, *J. Am. Chem. Soc.*, 2014, **136**, 16345–16356.

5 (*a*) C.-H. Wu, C.-C. Chueh, Y.-Y. Xi, H.-L. Zhong, G.-P. Gao, Z.-H. Wang, L. D. Pozzo, T.-C. Wen and A. K.-Y. Jen, *Adv. Funct. Mater.*, 2015, **25**, 5326–5332; (*b*) Y. Zhong, M. T. Trinh, R. Chen, G. E. Purdum, P. P. Khlyabich, M. Sezen, S. Oh, H. Zhu, B. Fowler, B. Zhang, W. Wang, C.-Y. Nam, M. Y. Sfeir, C. T. Black, M. L. Steigerwald, Y.-L. Loo, F. Ng, X.-Y. Zhu and C. Nuckolls, *Nat. Commun.*, 2015, **6**, 8242; (*c*) Q. Wu, D. Zhao, A. M. Schneider, W. Chen and L. Yu, *J. Am. Chem. Soc.*, 2016, **138**, 7248–7251; (*d*) N. Liang, K. Sun, Z. Zheng, H. Yao, G. Gao, X. Meng, Z. Wang, W. Ma and J. Hou, *Adv. Energy Mater.*, 2016, 1600060.

6 Y. Liu, J. Y. L. Lai, S. Chen, Y. Li, K. Jiang, J. Zhao, Z. Li, H. Hu, T. Ma, H. Lin, J. Liu, J. Zhang, F. Huang, D. Yu and H. Yan, *J. Mater. Chem. A*, 2015, **3**, 13632–13636.

7 (*a*) Y. Li, J. Gao, S. Di Motta, F. Negri and Z. Wang, *J. Am. Chem. Soc.*, 2010, **132**, 4208–4213; (*b*) Y. Li and Z. Wang, *Org. Lett.*, 2009, **11**, 1385–1387; (*c*) C. Li, C. Xiao, Y. Li and Z. Wang, *Org. Lett.*, 2013, **15**, 682–685; (*d*) J. Gao, Y. Li and Z. Wang, *Org. Lett.*, 2013, **15**, 1366–1369; (*e*) L. Tan, L. Zhang, X. Jiang, X. Yang, L. Wang, Z. Wang, L. Li, W. Hu, Z. Shuai, L. Li and D. Zhu, *Adv. Funct. Mater.*, 2009, **19**, 272–276.

8 H. Qian, W. Yue, Y. Zhen, S. Di Motta, E. Di Donato, F. Negri, J. Qu, W. Xu, D. Zhu and Z. Wang, *J. Org. Chem.*, 2009, **74**, 6275–6282.

9 Y. Zang, C.-Z. Li, C.-C. Chueh, S. T. Williams, W. Jiang, Z.-H. Wang, J.-S. Yu and A. K.-Y. Jen, *Adv. Mater.*, 2014, **26**, 5708–5714.

10 (*a*) D. Sun, D. Meng, Y. Cai, B. Fan, Y. Li, W. Jiang, L. Huo, Y. Sun and Z. Wang, *J. Am. Chem. Soc.*, 2015, **137**, 11156–11162; (*b*) D. Meng, D. Sun, C. Zhong, T. Liu, B. Fan, L. Huo, Y. Li, W. Jiang, H. Choi, T. Kim, J. Y. Kim, Y. Sun, Z. Wang and A. J. Heeger, *J. Am. Chem. Soc.*, 2016, **138**, 375–380.